The Fate of Close-in Planets: Tidal or Magnetic Migration?

A. Strugarek[1] , E. Bolmont[1], S. Mathis[1], A. S. Brun[1], V. Réville[1,2] , F. Gallet[3], and C. Charbonnel[3,4]
[1] Laboratoire AIM Paris-Saclay, CEA/Irfu Université Paris-Diderot CNRS/INSU, F-91191 Gif-sur-Yvette, France; antoine.strugarek@cea.fr
[2] UCLA Department of Earth, Planetary and Space Sciences, 595 Charles E. Young Drive East, Los Angeles, CA 90095, USA
[3] Department of Astronomy, University of Geneva, Chemin des Maillettes 51, 1290 Versoix, Switzerland
[4] IRAP, UMR 5277, CNRS and Université de Toulouse, 14, av. E. Belin, F-31400 Toulouse, France
Received 2017 September 1; revised 2017 September 15; accepted 2017 September 16; published 2017 September 27

Abstract

Planets in close-in orbits interact magnetically and tidally with their host stars. These interactions lead to a net torque that makes close-in planets migrate inward or outward depending on their orbital distance. We systematically compare the strength of magnetic and tidal torques for typical observed star–planet systems (T-Tauri and hot Jupiter, M-dwarf and Earth-like planet, K star and hot Jupiter) based on state-of-the-art scaling laws. We find that depending on the characteristics of the system, tidal or magnetic effects can dominate. For very close-in planets, we find that both torques can make a planet migrate on a timescale as small as 10–100 thousands of years. Both effects thus have to be taken into account when predicting the evolution of compact systems.

Key words: planet–star interactions – planets and satellites: dynamical evolution and stability – stars: magnetic field – stars: winds, outflows

1. Introduction

Thanks to space missions such as *CoRoT* (CoRot Team 2016), *Kepler* (Borucki et al. 2010), and *K2* (Howell et al. 2014) and ground-based observations (e.g., HARPS; Pepe et al. 2000), about 3000 exoplanets have been discovered as of today since the pioneering detection by Mayor & Queloz (1995). The corresponding planetary systems are very diverse in terms of planetary size and mass as well as orbital architecture. Due to the observational biases of the two most prolific detection techniques (transit and radial velocity), a majority of the detected exoplanets are close-in planets, which are very likely strongly interacting with their host star.

Star–planet interactions were proposed to have various effects on the dynamics and evolution of compact systems (Cuntz et al. 2000), among which angular momentum exchanges between the planet's orbit and the stellar spin (and to a lesser extent between the planet's orbit and the planet's spin). We concentrate here on the former, and we consider only planetary systems with one planet and no protoplanetary disk. These exchanges lead to the spin-up or spin-down of the star and the orbital migration of the planet due to two main physical processes: tidal and magnetic interactions (see Figure 1).

Tidal interactions consist of the gravitational response of a given body (here, the star) to a perturber (here, the planet) and its effect on rotation and orbit. There are two different components of the response: the hydrostatic non-wave-like equilibrium tide (e.g., Zahn 1966) and the dynamical tide. The dynamical tide can develop either in the radiative core of the star (e.g., Zahn 1975) or in its rotating convective envelope (e.g., Ogilvie & Lin 2007). The resulting dissipation can be several orders of magnitude higher than the dissipation due to the equilibrium tide (Ogilvie & Lin 2007; Bolmont & Mathis 2016), leading to a much faster orbital migration, especially for stars on the pre-main sequence (Bolmont & Mathis 2016; Gallet et al. 2017). Recent works on star–planet tidal interactions allowed us to give estimates of the dissipation due to the dynamical tide in the convective region of a star of a given mass, age, metallicity, and rotation (Bolmont et al. 2017; Gallet et al. 2017).

Simultaneously, magnetic interactions develop due to the differential motion between the planet and the magnetized ambient stellar wind at the planetary orbit. A net magnetic torque applies to the planet, effectively transferring angular momentum between the planet and star (if the planet is in the sub-Alfvénic region of the wind, close to the star), or between the planet and the ambient wind (if the planet is in the super-Alfvénic region of the wind). In the context of close-in planets, we consider here only the former interaction. Different regimes of the interaction occur depending on the magnetic properties of the planet (e.g., Zarka 2007; Strugarek et al. 2014). If the planet possesses an intrinsic magnetic field, the *dipolar* interaction develops (Saur et al. 2013; Strugarek et al. 2015; Strugarek 2016); otherwise, the interaction becomes *unipolar* (Laine & Lin 2012). The magnetic interaction between a star and a close-in planet can lead to many other notable effects such as anomalous emissions or planet inflation. A recent review on those effects can be found in Lanza (2017 and references therein).

In past studies about star–planet interactions, tides and magnetism have not been taken into account together, with the notable exception of Bouvier & Cébron (2015) in the context of young fast rotators. The aim of this Letter is thus to offer the first generic comparison of the strength of tidally induced versus magnetically induced orbital migration for typical compact star–planet systems. As a first step, we focus here on planets on a circular coplanar orbit. In Section 2, we estimate the migration timescales due to the tidal and the magnetic interactions. In Section 3, we compute the two migration timescales for three representative stars of different rotation and hosting planets of different orbital periods. We establish the parameter space for which tides or magnetism is the strongest driver of migration, and we give an example of three particular observed exoplanetary systems.
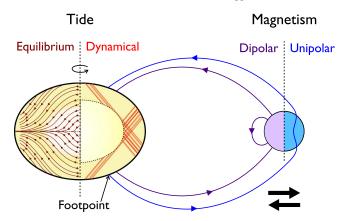
Figure 1. Sketch of the star–planet tidal and magnetic interactions. Only the tides (equilibrium tide and dynamical tide in the convective envelope) raised by the planet in the star are taken into account here. We consider both dipolar and unipolar magnetic interactions. Due to these interactions, the planet can migrate either inward or outward (black arrows).

2. Estimates of Torques Applied to Close-in Planets

We characterize the orbital migration of planets by the timescale defined as

$$\tau_{\mathrm{mig}} = \left| \frac{a}{\dot{a}} \right| = \frac{2J_P}{|\Gamma|}, \tag{1}$$

where Γ is the torque applied to the orbiting planet, $J_p = M_p \sqrt{GM_\star a}$ is the orbital angular momentum, M_p and $M_\star$ are the masses of the planet and the star, and a is the semimajor axis of the planet.

2.1. Tidal Torque

The torque associated with tidal dissipation in the host star leads to planet migration that scales as (Kaula 1964; Jackson et al. 2008)

$$|\Gamma_T| = 6J_p n \frac{M_p}{M_\star} \left(\frac{R_\star}{a} \right)^5 \frac{k_2}{Q_*}, \tag{2}$$

where $n = \sqrt{\frac{GM_\star}{a^3}}$ is the orbital frequency, $R_\star$ the stellar radius, k_2 the usual quadrupolar hydrostatic Love number, and Q_* the tidal dissipation quality factor.

Planets induce tidal flows in stars that have two components: the equilibrium and the dynamical tides. The equilibrium tide is a large-scale non-wave-like flow (e.g., Zahn 1966; Remus et al. 2012; Figure 1) sustained by the hydrostatic adjustment of the star because of the perturbation induced by a close planet. It is efficiently dissipated in the turbulent convective envelope of low-mass stars while its damping can be neglected elsewhere (Zahn 1977). However, this flow is not a complete solution of the hydrodynamics equations and it is completed by the so-called dynamical tide (Zahn 1975). In the convective envelope of late-type stars, the dynamical tide is constituted by inertial waves governed by the Coriolis acceleration and damped by the convective turbulent friction as in the case of the equilibrium tide (Ogilvie & Lin 2007). They are excited only when $n < 2\Omega_\star$ ($\Omega_\star$ is the stellar rotation rate). Mathis (2015b) demonstrated that their dissipation is efficient when a radiative core is present for sufficiently thick convective envelopes. This allows the formation of sheared wave attractors and an important enough volume where dissipation can take place.

In fully convective stars, for which attractors cannot form in the case of rigid rotation, and for $n > 2\Omega_\star$, only the equilibrium tide prevails. The dynamical tide can also occur in the radiative core (Zahn 1975; Ogilvie & Lin 2007), but in this first work, we will focus on the dissipation in the convective envelope only. We thus need an accurate estimate of $k_2/Q_\star$ for each type of tide.

2.1.1. Equilibrium Tide

The dissipation of the equilibrium tide can be estimated using the analytical model developed by Remus et al. (2012). In this model, the tidal dissipation is written as

$$\frac{k_2}{Q_*} = 4\pi \frac{2088}{35} \frac{R_\star^4}{GM_\star^2} \left| \sigma \int_\alpha^1 x^8 \rho \nu_t \, dx \right|, \tag{3}$$

where $\sigma = 2(n - \Omega_\star)$ is the tidal frequency in the coplanar circular case studied here, ν_t the turbulent viscosity in the convection zone, $\alpha = R_{bcz}/R_\star$, R_{bcz} being the radius of its base, ρ the density in the convection zone, and $x = r/R_\star$ the normalized radial coordinate. We derive hereafter an estimate of Equation (3) based only on the global parameters of the system.

The turbulent viscosity strength depends on how the convective turnover time t_c compares to the tidal frequency σ. Following Zahn (1966) and Remus et al. (2012), we can generically write

$$\nu_t = \frac{1}{3} v_c l_c \left[1 + \left(\frac{t_c \sigma}{\pi} \right)^2 \right]^{-1/2}, \tag{4}$$

where v_c is the typical convective velocity and l_c is the mixing length. These three parameters can be estimated using the derivation from Mathis et al. (2016) based on the mixing-length theory for a rotating body (proposed in Stevenson 1979 and validated by recent high-resolution numerical simulations; Barker et al. 2014). We define the convective Rossby number as $R_o^c = t_\Omega / t_c^0$ (t_Ω being the rotation period of the star and t_c^0 the convective turnover time from the standard mixing-length theory that neglects rotation), and use the following estimates (Mathis et al. 2016):

$$v_c \simeq \left(\frac{L_\star}{\bar{\rho}_{\mathrm{CZ}} R_\star^2} \right)^{1/3} \times \begin{cases} \left(1 - \dfrac{1}{242(R_o^c)^2} \right) & \text{if } R_o^c > 0.25 \\ 1.5(R_o^c)^{1/5} & \text{if } R_o^c < 0.25 \end{cases}, \tag{5}$$

$$l_c \simeq \alpha_{\mathrm{MLT}} H_P \times \begin{cases} \left(1 + \dfrac{1}{82(R_o^c)^2} \right)^{-1} & \text{if } R_o^c > 0.25 \\ 2(R_o^c)^{3/5} & \text{if } R_o^c < 0.25 \end{cases}, \tag{6}$$

$$t_c = \frac{l_c}{v_c}, \tag{7}$$

where we have introduced the stellar luminosity $L_\star$, the average density in the convection zone $\bar{\rho}_{\mathrm{CZ}}$, the mixing-length parameter α_{MLT}, and the pressure scale height H_P. Given that we aim here for an order of magnitude estimate, we perform further approximations that $\rho = \bar{\rho}_{\mathrm{CZ}}$ and that ν_t in the integral in Equation (3) do not vary with depth. Furthermore, we approximate the mixing length l_c by its maximum, which is

given by the depth of the convection zone $(1 - \alpha)R_\star$. We set $\bar{\rho}_{CZ} = 3M_\star(1 - \beta)/4\pi R_\star^3(1 - \alpha^3)$ to the density of the convective envelope, with $\beta = M_{bcz}/M_\ast$ (M_{bcz} is the radiative core mass). We finally obtain

$$\frac{k_2}{Q_\ast} \simeq \frac{232}{35} \frac{|t_c\sigma|}{\sqrt{1 + \left(\frac{t_c\sigma}{\pi}\right)^2}} \frac{R_\star}{GM_\star} v_c^2 (1 - \beta) \frac{1 - \alpha^9}{1 - \alpha^3}. \qquad (8)$$

2.1.2. Dynamical Tide: Tidal Inertial Waves

The case of tidal inertial waves excited in the convective envelope of low-mass stars is complex to treat. As demonstrated by Ogilvie & Lin (2007), the induced tidal torque strongly depends on the tidal frequency and can vary over several orders of magnitude as a function of the stellar mass, age, metallicity, rotation, and turbulent viscosity. Hence, a coherent treatment of this tidal dissipation requires the coupling of hydrodynamical numerical codes to compute tidal inertial waves (e.g., Guenel et al. 2016), and rotational and orbital evolution codes to take into account their dissipation along the evolution planetary systems (e.g., Bolmont et al. 2015; Bolmont & Mathis 2016). An alternative approach has been proposed by Ogilvie (2013) and Mathis (2015b, 2015a), who estimated the order of magnitude of the friction induced by the dissipation of tidal inertial waves thanks to analytical frequency-averaged dissipation rates derived using spherical bi-layer rotating stellar structure models. They obtain

$$\frac{k_2}{Q_\ast} = \frac{100\pi}{63}\epsilon^2 \frac{\alpha^5(1 - \gamma)^2}{1 - \alpha^5}$$

$$\times \frac{(1 - \alpha)^4\left(1 + 2\alpha + 3\alpha^2 + \frac{3}{2}\alpha^3\right)^2\left(1 + \frac{1 - \gamma}{\gamma}\alpha^3\right)}{\left[1 + \frac{3}{2}\gamma + \frac{5}{2\gamma}\left(1 + \frac{1}{2}\gamma - \frac{3}{2}\gamma^2\right)\alpha^3 - \frac{9}{4}(1 - \gamma)\alpha^5\right]^2}, \qquad (9)$$

where $\gamma = \frac{\alpha^3(1 - \beta)}{\beta(1 - \alpha^3)}$ and $\epsilon = \Omega_\star/\Omega_{\rm kep}(R_\star)$ with the Keplerian rotation rate $\Omega_{\rm kep}(r) = \sqrt{GM_\star/r^3}$. In this work, we use the stellar evolution grid of Gallet et al. (2017)[5] to estimate α and β for a given star.

2.2. Magnetic Torque

2.2.1. Stellar Wind Model

The magnetic interaction in compact star–planet systems depends on the local properties of the stellar wind at the planetary orbit. In order to estimate these properties, we use the simple 1D magnetized wind model *starAML* (see Réville et al. 2015 for a complete description; the code is available upon request from the authors). This model solves the pressure balance of a magnetized 1D Parker-like wind (Parker 1958; Weber & Davis 1967; Sakurai 1985). The magnetic field of the wind is extrapolated with a potential field with a source surface (Schatten et al. 1969) calibrated over 2D and 3D numerical simulations of stellar winds (see Réville et al. 2016 for 3D). The general properties of the wind such as velocity, mass and angular momentum loss rates, and Alfvén radius are then simply computed. In the present work, we assume a ratio of specific heats $c_p/c_v = 1.05$, which mimics the coronal heating and allows us to reproduce the solar wind with this model. We scale the density and temperature at the base

of the corona with the rotation rate of the star using the observational prescription of Holzwarth & Jardine (2007). The large-scale magnetic field of the star B_s is assumed to depend on the rotation rate of the star as

$$B_s = B_\star \begin{cases} 1 & \text{if } R_o^c < 0.25 \\ \left(\frac{R_o^c}{0.25}\right)^{-1.38} & \text{if } R_o^c > 0.25 \end{cases}, \qquad (10)$$

where the exponent -1.38 is taken from the empirical trend found by Vidotto et al. (2014), and $B_\star$ is the reference stellar field in the rotationally saturated regime ($R_o^c < 0.25$). We choose here a threshold at $R_o^c = 0.25$ to be consistent with the threshold for tides (see Section 2.1.1), which is close to the observationally constrained saturation value (e.g., Gondoin 2012; Vidotto et al. 2014).

With this wind model, we can furthermore infer whether the planet is able to sustain a magnetosphere for a given planetary magnetic field surface amplitude B_p. In this work, we consider a dipolar or an unipolar regime of interaction depending whether or not a magnetosphere can be sustained (see Figure 1).

2.2.2. Unipolar Interaction

In cases where the ambient pressure from the stellar wind is too strong, the planet magnetic field may not be strong enough to sustain a magnetosphere. In this case, the magnetic interaction in a close-in system becomes unipolar and was studied by Laine et al. (2008) and Laine & Lin (2012). The magnetic torque can then be written as

$$|\Gamma_M| = 8R_p^2 a^2|\sigma|\, B_w\Sigma, \qquad (11)$$

where R_p is the planet radius, B_w is the stellar wind magnetic field at the planetary orbit, and Σ is the resistance of the stellar plasma at the footpoint of the interaction (see Figure 1) that was estimated to be of the order of $6.5 \times 10^{-6}\,{\rm s\,cm^{-1}}$ by Laine & Lin (2012). Note that we have simplified the original equation to neglect the dependency of the torque to the incidence angle of the interaction footpoint at the stellar surface for the sake of simplicity. The torque (11) was derived assuming a rocky super-Earth planet in Laine & Lin (2012) and is valid as long as ohmic dissipation is more efficient at the footpoint of the interaction at the stellar surface than inside the planet itself. This assumption may also hold for gaseous planets, depending on their poorly constrained conductivity profile in their interior (e.g., Umemoto et al. 2006; van den Berg et al. 2010). We suppose here that Equation (11) holds for all planets considered, but warn the reader that the unipolar torque may decrease if the conductivity inside the planet is comparable to or less than the conductivity at the stellar surface.

2.2.3. Dipolar Interaction

The torque Γ_M associated with magnetic forces has been modeled in Strugarek et al. (2015) and Strugarek (2016) when the planet possesses a magnetosphere (the so-called dipolar regime). It can be parameterized as

$$|\Gamma_M| = A_0\pi(c_d P_t M_a^\chi) \cdot (R_p^2 a)\Lambda_p^\xi, \qquad (12)$$

Table 1
Representative Systems

Star–Planet System	$M_\star$ ($M_\odot$)	$R_\star$ ($R_\odot$)	$B_\star$ (G)	α^a	β^a	$T_{eff}{}^a$ (K)	M_p ($M_\oplus$)	R_p ($R_\oplus$)	P_{orb} (days)	B_p (G)	Analog System
T-Tauri + hot Jupiter	1.05	1.12	2500	0.583	0.728	4475	318	11	10.9	10	Tap-26 (b)[b]
M dwarf + Earth	0.13	0.17	1000	0	0	3070	0.3	0.7	0.45	1	Kepler–42 (c)[c]
K star + hot Jupiter	0.80	0.80	140	0.672	0.929	4875	363	12.5	2.2	28[e]	HD 189733 (b)[d]

Note. The stellar parameters (a) are taken from Gallet et al. (2017). The planet parameters are derived from Yu et al. (2017) (b), Muirhead et al. (2012) (c), and Bouchy et al. (2005) (d). The magnetic field of the star and the planet are assumed here, except for the third system (e) for which we took the value inferred by Cauley et al. (2015) using observed abnormal pre-transit absorptions to estimate the size of the planet's hypothetical magnetosphere.

where P_t is the stellar wind total pressure at the planetary orbit, M_a the Alfvénic Mach number, and Λ_p the pressure ratio between the magnetic pressure in the magnetosphere of the planet and the wind pressure P_t. The coefficients A_0, χ, and ξ have been calibrated from a set of 3D numerical simulations in Strugarek (2016) and depend on the magnetic topology of the interaction. We will consider in this Letter only the aligned configuration, which maximizes the magnetic torque. Note that we also omitted the dependency of the torque to the resistive properties of the wind plasma for the sake of simplicity (see Strugarek 2016 for a complete discussion). Finally, we assume that the planet magnetic field B_p is independent of the spin of the planet (and hence of its orbital period in tidally locked systems). This is a reasonable approximation, as we expect the magnetic moment of a planet to depend only weakly on its rotation rate (Christensen 2010; Davidson 2013).

3. Application to Particular Star–Planet Systems

Our goal is to compare the instantaneous timescales associated with tidal and magnetic forces (Equation (1)). We thus define their ratio as

$$\Xi = \frac{\tau_T}{\tau_M}, \tag{13}$$

where the tidal (τ_T) and magnetic (τ_M) migration timescales are defined by Equation (1) with the torque Γ_T defined by (2) for tides, and Γ_M by (11) or (12) for magnetism. The overall migration timescale due to the sum of tidal and magnetic torques $\Gamma_T + \Gamma_M$ can be written as

$$\tau = \frac{\tau_T \tau_M}{\tau_T + \tau_M}. \tag{14}$$

The migration timescale formulae in Section 2 are generic to star–planet close-in systems. We now apply them to three illustrative systems listed in Table 1.

We first consider the case of a T-Tauri star like Tap-26 (Yu et al. 2017), with a surrounding hot Jupiter possessing a magnetic field twice as strong as Jupiter's. The T-Tauri is a young solar-like star that is assumed here to generate a strong surface magnetic field of the order of 2500 G (e.g., Donati & Landstreet 2009). The resulting tidal and magnetic migration timescales are shown in the left column of Figure 2 as a function of the rotation period of the star and the orbital period of the planet (the Tap-26 system is labeled by the orange circle).

The isocontours of the tidal migration timescale are shown in Figure 2(A). The gray area masks regions where the torque is too weak and the associated migration timescale is larger than the age of the universe. The different regimes of the tidal

migration efficiency clearly appear in this panel. A sharp transition is observed at $n = 2\Omega_\star$ (oblique black dashed line): the dynamical tide (red) operates only in star–planet systems below this transition line, dramatically improving the efficiency of the tidal dissipation. A second transition is observed in the equilibrium tide region above (dark red), labeled by the horizontal black line with long dashes, where the star enters a large Rossby number regime (see Section 2.1.1). In the upper part of the diagram, the tidal migration timescale becomes essentially independent of the slow rotation rate of the star, as expected. The black oblique line represents the corotation radius: a planet below this line migrates outward and a planet above this line migrates inward.

The magnetic migration timescale is shown in Figure 2(B). Because the Alfvén surface of the wind is located farther than a 10 day orbit, the wind is assumed here to be in corotation with the star, meaning that the corotation line is the same here as for tides. We suppose that the planet possesses an intrinsic surface magnetic field of 10 G. A sharp transition occurs at 0.9 days (black dashed–dotted line) as the magnetic interaction changes from dipolar (dark blue) to unipolar (blue). The latter is shown to be more efficient than the effective drag occurring in the dipolar interaction case.

The ratio between the two timescales Ξ is shown in Figure 2(C). The thick black contour labels the positions where the tidal and magnetic torques have the same amplitude. Red (blue) regions denote regions where the tidal (magnetic) torque dominates. We note that, generally, tidal effects dominate in the regions where dynamical tides operate. For slowly rotating systems, though, both torques are clearly comparable with one slightly dominating the other depending on the orbital period of the planet.

Finally, the overall migration timescale τ is shown in logarithmic scale in Figure 2(D). The closest planets migrate on a timescale of several thousands of years due to both tidal and magnetic torques for most stellar rotation rates. Both torques strongly decrease with the orbital distance. As a result, planets with orbital periods longer than 10 days are essentially insensitive to tidal and magnetic torques.

Figure 2(E)–(H) show the same quantities for a fully convective M dwarf resembling Kepler–42 (Muirhead et al. 2012, the orange circle labels Kepler–42 c). In this case, the dynamical tide is much less efficient as there are no attractors, and as a result the tidal migration timescale is long for all rotation rates. The torque applied to close-in planets is completely dominated by magnetic effects, due to both the weak tidal torque and the relatively strong magnetic field of the M dwarf. The critical period at which the star reaches a Rossby number of 0.25 is 28 days in this case. Because of the relatively weak magnetic field of the planet, the magnetic interaction mostly develops in a unipolar regime in such systems. Only
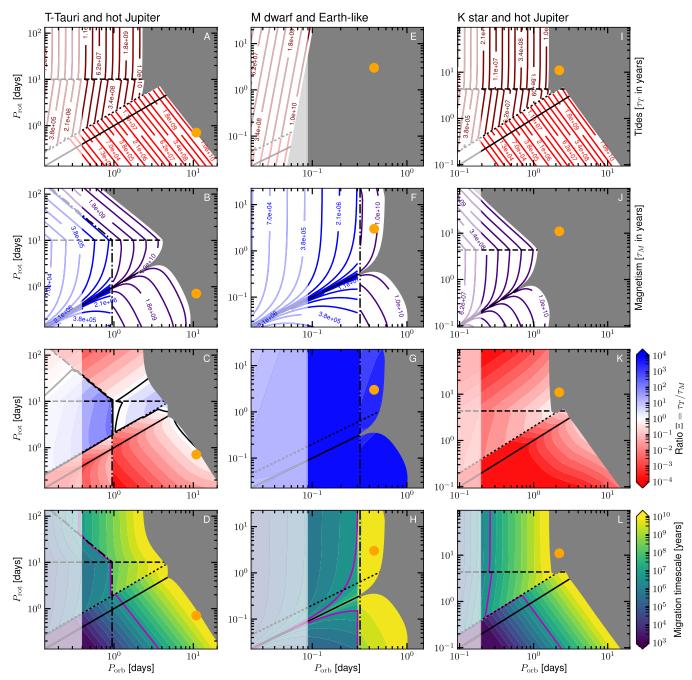
Figure 2. Tidal and magnetic torques in three representative star–planet systems (each column represents one system). The tidal (first row: (A), (E), (I)) and magnetic (second row: (B), (F), (J)) migration timescales are contoured with labels in years. The ratio between the tidal and magnetic migration timescales is shown in the third row ((C), (G), (K)), with blue (red) denoting magnetic (tidal) dominance. The overall migration timescale is displayed in logarithmic scale in the bottom row ((D), (H), (L)). The magenta line corresponds to a timescale of 5 Myr, which is representative of a stellar structure evolution timescale on the pre-main sequence. All panels are shown as a function of the rotation period of the star and the orbital period of the planet, in days. The gray area masks regions where the migration timescale is larger than the age of the universe. The Roche limit is labeled by the white transparent area and calculated as in Strugarek et al. (2014). The orange circles label the position of the three analog systems identified in Table 1. The oblique black lines label corotation (solid line) and dynamical tide transition (dashed line). The horizontal black line with long dashes labels the transition at $R_o^c = 0.25$, and the dashed–dotted line traces the change of magnetic interaction regime.

planets with orbital periods smaller than ∼0.3 days are expected to significantly migrate.

Finally, we study in Figures 2(I)–(L) the case of an evolved K star with a close-in hot Jupiter like HD 189733 (Bouchy et al. 2005, the orange circle labels HD 189733 b). The magnetic field of the star is much weaker than in the two previous cases, and the tidal torque completely dominates the migration path of the close-in planet (Figure 2(K)). We immediately see that for the HD 189733 system, it is unlikely

that the tidal and magnetic torques studied in this work can make the planet migrate significantly. Indeed, only planets with orbital periods smaller than ∼2 days are expected to migrate in such a system.

4. Discussion and Conclusions

Magnetic and tidal effects generally act together in close-in systems to make planets migrate inward or outward. We found

that both effects can dominate depending on the star–planet system considered. Magnetic effects are likely to dominate when the dynamical tide is not operating (e.g., for fully convective stars) and when the stellar magnetic field is strong. The overall torque depends on many parameters of the star–planet system, such as the stellar structure, its magnetic field, and rotation rate and the planet orbital distance, its structure, and its internal magnetic field. The multiple dependencies of the torques are fully accounted for in the simple scaling laws we summarized in this Letter. When considering particular systems for which some parameters are not available, a simple parameter space exploration rapidly gives minimal and maximal migration timescale that can be attained due to tides and magnetic fields.

We have applied these scaling laws to three representative systems (Figure 2). We found that very close-in planets could migrate on a timescale as small as tens to hundreds of thousands of year due to the combination of tidal and magnetic interactions with their host. This migration timescale is short and renders the detection of such systems statistically unlikely. The observation of systems for which the magnetic or tidal torques are strong would provide a fantastic test-bed for the estimates we derived in this Letter. For the three systems studied here, the known planets lie in a region of a very long migration timescale (orange disks). In the particular case of HD 189733, this suggests that no significant angular momentum transfer between HD 189733 b and its host is occurring due to either magnetic or tidal interactions.

We have considered isolated, tidally locked planets on a coplanar circular orbit. While this may be a reasonable assumption for single-planet systems, it is not realistic for multiple-planet systems. The tidal torque scaling laws should be derived in the case of elliptic systems (e.g., using Kaula 1961), but more theoretical work is still needed to develop estimates of the magnetic torques in such systems. The friction induced by the damping of tidal gravity waves in the radiative core of low-mass stars (Zahn 1975) should also be taken into account in a near future, as well as tidal elliptic instabilities (Cébron et al. 2013).

In the context of young star–planet systems, we have also neglected the contributions from interactions with a disk. Planet migration in a disk through Lindblad resonances is generally thought to be more efficient than the effects considered in this work (e.g., Baruteau et al. 2014; Bouvier & Cébron 2015). We note though that the migration due to self-consistent dynamical tides was not systematically compared to disk-induced migration, which we leave for future work.

Finally, we recall that we have focused our discussion on order of magnitude estimates of instantaneous migration timescales. The scaling laws summarized in this Letter could also be implemented in stellar and orbital evolution codes (Zhang & Penev 2014; Bolmont et al. 2015; Gallet et al. 2017) to evolve self-consistently the star and its orbiting planet over secular timescales, in particular when the migration timescale is longer than the characteristic evolution time of the star (see, e.g., the magenta line in Figure 2). For older stars such as the M dwarf and K star studied here, the stellar parameters are not expected to change significantly during their evolution over the main sequence, and our instantaneous estimates already provide a good approximation of the migration path of close-in planets.

As a general conclusion, stars and close-in planets are interacting both through gravitational and electromagnetic interactions and both of them should be taken into account to predict their evolution.

ORCID iDs

A. Strugarek ● https://orcid.org/0000-0002-9630-6463
V. Réville ● https://orcid.org/0000-0002-2916-3837

References

Barker, A. J., Dempsey, A. M., & Lithwick, Y. 2014, ApJ, 791, 13
Baruteau, C., Crida, A., Paardekooper, S. J., et al. 2014, in Protostars and Planets VI, ed. H. Beuther et al. (Tucson, AZ: Univ. Arizona Press), 667
Bolmont, E., Gallet, F., Mathis, S., et al. 2017, A&A, 604, A113
Bolmont, E., & Mathis, S. 2016, CeMDA, 126, 275
Bolmont, E., Raymond, S. N., Leconte, J., Hersant, F., & Correia, A. C. M. 2015, A&A, 583, A116
Borucki, W. J., Koch, D., Basri, G., et al. 2010, Sci, 327, 977
Bouchy, F., Udry, S., Mayor, M., et al. 2005, A&A, 444, L15
Bouvier, J., & Cébron, D. 2015, MNRAS, 453, 3720
Cauley, P. W., Redfield, S., Jensen, A. G., et al. 2015, ApJ, 810, 13
Cébron, D., Bars, M. L., Gal, P. L., et al. 2013, Icar, 226, 1642
Christensen, U. R. 2010, SSRv, 152, 565
CoRot Team 2016, The CoRoT Legacy Book: The Adventure of the Ultra High Precision Photometry from Space, ed. C. Team & A. Baglin (Les Ulis: EDP Sciences)
Cuntz, M., Saar, S. H., & Musielak, Z. E. 2000, ApJL, 533, L151
Davidson, P. A. 2013, GeoJ, 195, 67
Donati, J.-F., & Landstreet, J. D. 2009, ARA&A, 47, 333
Gallet, F., Bolmont, E., Mathis, S., Charbonnel, C., & Amard, L. 2017, A&A, 604, A112
Gondoin, P. 2012, A&A, 546, A117
Guenel, M., Baruteau, C., Mathis, S., & Rieutord, M. 2016, A&A, 589, A22
Holzwarth, V., & Jardine, M. 2007, A&A, 463, 11
Howell, S. B., Sobeck, C., Haas, M., et al. 2014, PASP, 126, 398
Jackson, B., Greenberg, R., & Barnes, R. 2008, ApJ, 678, 1396
Kaula, W. M. 1961, GeoJ, 5, 104
Kaula, W. M. 1964, RvGSP, 2, 661
Laine, R. O., & Lin, D. N. C. 2012, ApJ, 745, 2
Laine, R. O., Lin, D. N. C., & Dong, S. 2008, ApJ, 685, 521
Lanza, A. F. 2017, The Handbook of Exoplanets, in press
Mathis, S. 2015a, in SF2A-2015: Proceedings of the Annual Meeting of the French Society of Astronomy and Astrophysics, ed. F. Martins, 401
Mathis, S. 2015b, A&A, 580, L3
Mathis, S., Auclair-Desrotour, P., Guenel, M., Gallet, F., & Le Poncin-Lafitte, C. 2016, A&A, 592, A33
Mayor, M., & Queloz, D. 1995, Natur, 378, 355
Muirhead, P. S., Hamren, K., Schlawin, E., et al. 2012, ApJL, 750, L37
Ogilvie, G. I. 2013, MNRAS, 429, 613
Ogilvie, G. I., & Lin, D. N. C. 2007, ApJ, 661, 1180
Parker, E. N. 1958, ApJ, 128, 664

Pepe, F., Mayor, M., Delabre, B., et al. 2000, Proc. SPIE, 4008, 582
Remus, F., Mathis, S., & Zahn, J.-P. 2012, A&A, 544, 132
Réville, V., Brun, A. S., Matt, S. P., Strugarek, A., & Pinto, R. F. 2015, ApJ, 798, 116
Réville, V., Folsom, C. P., Strugarek, A., & Brun, A. S. 2016, ApJ, 832, 145
Sakurai, T. 1985, A&A, 152, 121
Saur, J., Grambusch, T., Duling, S., Neubauer, F. M., & Simon, S. 2013, A&A, 552, 119
Schatten, K. H., Wilcox, J. M., & Ness, N. F. 1969, SoPh, 6, 442
Stevenson, D. J. 1979, GAFD, 12, 139
Strugarek, A. 2016, ApJ, 833, 140
Strugarek, A., Brun, A. S., Matt, S. P., & Réville, V. 2014, ApJ, 795, 86
Strugarek, A., Brun, A. S., Matt, S. P., & Réville, V. 2015, ApJ, 815, 111
Umemoto, K., Wentzcovitch, R. M., & Allen, P. B. 2006, Sci, 311, 983
van den Berg, A. P., Yuen, D. A., Beebe, G. L., & Christiansen, M. D. 2010, PEPI, 178, 136
Vidotto, A. A., Gregory, S. G., Jardine, M., et al. 2014, MNRAS, 441, 2361
Weber, E. J., & Davis, L. J. 1967, ApJS, 148, 217
Yu, L., Donati, J.-F., Hébrard, E. M., et al. 2017, MNRAS, 467, 1342
Zahn, J.-P. 1966, AnAp, 29, 489
Zahn, J.-P. 1975, A&A, 41, 329
Zahn, J.-P. 1977, A&A, 57, 383
Zarka, P. 2007, P&SS, 55, 598
Zhang, M., & Penev, K. 2014, ApJ, 787, 131